Geophysical Journal International

Geophys. J. Int. (2010) **183,** 695–705 doi: 10.1111/j.1365-246X.2010.04786.x

GJI Geomagnetism, rock magnetism and palaeomagnetism

Superparamagnetism of two modern soils from the northeastern Pampean region, Argentina and its paleoclimatic indications

Qingsong Liu,[1] José Torrent,[2] Héctor Morrás,[3] Ao Hong,[1]* Zhaoxia Jiang[1] and Youliang Su[1,4]

[1]*State Key Laboratory of Lithospheric Evolution (SKL-LE), Institute of Geology and Geophysics, Chinese Academy of Sciences, Beijing* 100029, *China. E-mail: qsliu@mail.iggcas.ac.cn*
[2]*Departamento de Ciencias y Recursos Agrícolas y Forestales, Universidad de Córdoba, Edificio* C4, *Campus de Rabanales,* 14071 *Córdoba, Spain*
[3]*Instituto de Suelos, Centro de Investigación de Recursos Naturales, INTA,* 1618 *Hurlingham, Buenos Aires, Argentina*
[4]*Institute of Tibetan Plateau Research, Chinese Academy of Sciences, Beijing* 100085, *China*

Accepted 2010 August 20. Received 2010 August 16; in original form 2010 January 19

SUMMARY

The magnetic susceptibility (χ) carried by pedogenic fine-grained ferrimagnets has been widely used as paleoclimatic proxy to elucidate long-term paleoclimatic variations for wind-blown terrestrial loess/paleosol sequences. However, the magnetic properties of the lithogenic parent material can mask the pedogenic signals. In this study, we systematically investigated the origin of the superparamagnetism of two modern soils from the northeastern humid Pampean region, Argentina, developed on loess materials of different mineralogical composition. The samples were treated with the citrate–bicarbonate–dithionite (CBD) reagent, which is known to dissolve the submicron, pedogenic ferrimagnets while leaving unaltered the coarse grained ones. The magnetic material accounting for the frequency-dependent magnetic susceptibility peak at about 50 K remained in the residuals and is independent of the pedogenic processes. In addition, pedogenic ferrimagnetic particles in the two soils have a magnetic signature comparable to that of the soils from the Chinese Loess Plateau. It is also suggested that the χ for the bulk samples does not seem to be a reliable paleoclimatic proxy for the Pampean soils investigated in this study. Instead, the CBD-soluble magnetic signals could be more useful to detect paleoenvironmental variations in this region. These new findings provide improved understanding of the magnetic assemblage in the Pampean loess soils and make it feasible to retrieve the paleoclimatic signals carried by the pedogenic, CBD-soluble, iron oxides after removing the effects of the lithogenic inputs.

Key words: Rock and mineral magnetism.

1 INTRODUCTION

The formation of wind-blown loess deposits is sensitive to paleoclimatic variations and thus intensive studies have been conducted on the loess/paleosol sequences around the world, for example, the Chinese Loess Plateau (Heller & Liu 1984, 1986; Liu 1985; Kukla *et al*. 1988; Liu & Ding 1998; Ding *et al.* 2002), Siberia (Volkov & Zykina. 1982; Chlachula *et al.* 1997, 1998; Kravchinsky *et al.* 2008), Europe (Shi *et al.* 2001; Bugglea *et al.* 2008), Alaska (Lagroix & Banerjee 2004a,b), Midwestern United States (Geiss & Zanner 2006) as well as Argentina (Orgeira *et al*. 1998, 2003, 2008; Nabel *et al*. 1999; Bidegain *et al.* 2001; Bidegain & Rico 2004; Bidegain *et al*. 2005, 2009). Among these terrestrial paleoclimatic archives, the Chinese loess provides the longest records (Heller & Liu 1984, 1986; Liu 1985). During cold periods, aeolian materials were transported by the Asian winter monsoon and were deposited on the Chinese Loess Plateau at a relatively high sedimentation rate. During warm periods, aeolian accretions were reduced and soils developed on the loess. Pedogenesis then resulted in the formation of iron oxides, including hematite, goethite and nano-sized maghemite/magnetite, the latter being mostly responsible for the magnetic properties of Chinese paleosols (Zhou *et al.* 1990; Liu *et al*. 2005).

This model cannot, however, be generalized to loess deposits from other regions, specifically those from Siberia, Alaska and Argentina. Studies on the Siberia and Alaska loesses showed that the paleosols have weaker magnetic signals than the loess units (Begét & Hawkins 1989; Evans *et al*. 2003; Lagroix & Banerjee 2004a,b). Possible reasons are that the magnetic properties of the samples are controlled by the grain size variations in the aeolian magnetite rather than by the concentration of pedogenic magnetic particles (Begét *et al*. 1990; Begét 1996; Chlachula *et al.* 1997, 1998) or that the pedogenic ferrimagnets were reductively dissolved

*Now at: State Key Laboratory of Loess and Quaternary Geology, Institute of Earth Environment, Chinese Academy of Sciences, Xian 710075, China.

when soils were water-logged (Maher 1998; Bloemendal & Liu 2005). The lower magnetic susceptibility of the paleosol units in the Argentina loess/paleosol sequences has also been attributed to dissolution processes (Orgeira *et al.* 1998, 2003, 2008; Bidegain *et al*. 2009) although the causes of the magnetic variations of the Argentina loess still remain elusive (Nabel *et al*. 1999; Bidegain *et al*. 2005).

So far, most studies on the Argentina loess focus on the materials from the Pampean plain, which is one of the largest loess regions in the world (Teruggi 1957; Zárate 2003). The deposits from this region are characterized by low values of frequency-dependent magnetic susceptibility (χ_{fd} per cent $= 100 \times \chi_{fd}/\chi_{lf}$, where $\chi_{fd} = \chi_{lf} - \chi_{hf}$ and χ_{lf} and χ_{hf} are magnetic susceptibilities measured at low and high frequencies, respectively), which, as discussed below, is an indicator of the presence of submicron grains near the superparamagnetic (SP)-–stable single domain (SSD) threshold. By contrast, many other natural soil samples have relatively higher χ_{fd} per cent values of up to ~15 per cent (Stephenson 1971; Mullins & Tite 1973; Mullins 1977; Oldfield *et al*. 1985; Dearing *et al*. 1996; Morrás *et al*. 2009).

Worm (1998) showed that χ_{fd} per cent for SP particles depends greatly on grain size distribution (GSD). Only the χ of the viscous SP (VSP) particles located near the SP and SSD threshold is frequency-dependent. For example, high (>30 per cent) χ_{fd} per cent values have been observed for fine-grained magnetic particles with narrow GSDs around the SP/SSD threshold in tuffs from Yucca Mountain (Worm & Jackson 1999). In contrast, generally, χ of both stable SSD and extremely fine-grained SP particles is frequency-independent at room temperature. Therefore, the presence of SSD and extremely fine-grained SP particles strongly affect the χ_{fd} per cent values at room temperature (Worm & Jackson 1999).

Orgeira *et al*. (2003) measured the low-temperature (<300 K) temperature-dependence of χ_{fd} for a representative paleosol sample (TQ56) below a recent sediment from the Chacopampean region and observed frequency-dependent behaviour below 100 K, which corresponds to SP particles with a diameter of 13–16 nm. Vasquez *et al*. (2009) also suggested the presence of such fine-grained (12–16 nm) SP particles using the low-temperature thermal demagnetization of saturation isothermal remanent magnetization (SIRM) curves. In addition, coarser-grained ferrimagnetic particles of lithogenic origin were also confidently identified in Argentinian soils (Nabel *et al*. 1999; Orgeira *et al*. 2003; Bartel 2009). Therefore, the grain sizes of ferrimagnetic particles from these samples are dominated by two end-members, extremely fine-grained SP particles and coarse-grained particles of lithogenic origin.

However, the origin of the SP particles remains unclear. Orgeira *et al*. (2003) proposed that the ferrimagnetic particles in Argentinian paleosols first underwent dissolution and that the extremely fine-grained SP particles were formed at a later stage, for example, from inorganic processes in adequate soil pH and Eh (Vasquez *et al*. 2009). If so, the presence of these SP particles could indicate that the climate had a wet season (when soil Fe oxides were reductively dissolved) and a dry season (when new Fe oxides were formed). The Argentina loess is dominantly of volcanic-pyroclastic origin (Teruggi 1957) and has been formerly considered relatively homogeneous from a mineralogical point of view, particularly concerning the composition of its clay fraction. Nevertheless, several studies show a heterogeneous mineralogical composition in the coarse and fine fractions of loessic sediments from diverse areas in the Pampa region (Morrás & Delaune 1985; Morrás *et al*. 2002; Morrás 2003; Etchichury & Tófalo 2004; Castiglioni *et al.* 2007), together with clear differences in their geochemical composition (Morrás *et al*. 1998a,b; Morrás 1999; Morrás & Cruzate, 2002). These heterogeneities of loessian pampean sediments could derive from the existence of different source areas whose relative contributions vary across the region (Morrás 1999, 2003; Zárate 2003). Therefore, the origin of the SP particles, whether pedogenic or lithogenic, remains unclear without further systematic mineral magnetic studies.

Several authors have studied the magnetic properties of soil/paleosol sequences on loess deposits in the Argentinian Pampa (Orgeira *et al*. 1998, 2003; Nabel *et al*. 1999; Bidegain *et al*. 2001, 2005; Orgeira & Compagnucci 2006; Orgeira *et al*. 2008). Their results show that the magnetic susceptibility of the loess/paleosol sequences has a trend opposite to that of the Chinese loess, as is the case with the aforementioned Siberian and Alaskan deposits. In contrast, the modern soil has enhanced magnetic properties in the B horizons that resemble those of modern soil profiles in other regions. This suggests pedogenic formation of ferrimagnets rather than dissolution under reducing conditions of the ferrimagnets present in the parent loess.

This paper examines the magnetic properties of two modern soil profiles from the northeastern (humid) Pampean region developed on loessic materials differing in their mineralogical composition. Unlike previous studies on bulk samples, the pedogenic and lithogenic magnetic signals were separated by comparing the properties of the raw samples with those of samples treated with a citrate–bicarbonate–dithionite (CBD) solution. This solution (Mehra & Jackson 1958) is a reducing reagent that selectively dissolves Fe oxides (a term that is used here to designate all Fe(III) oxides, hydroxides and oxyhydroxides) of submicron size but it cannot dissolve magnetite/maghemite grains larger that about 1 μm to a significant extent (Hunt *et al*. 1995). Because only a small proportion of the magnetite/maghemite grains in unweathered loess are smaller than 1 μm (e.g. Chen *et al*. 2005) the CBD treatment results in a small loss of the lithogenic χ signal (Verosub *et al.* 1993; Singer *et al.* 1995; Sun *et al*. 1995; van Oorschot & Dekkers 1999; Vidic *et al*. 2000; Deng *et al*. 2005).

In summary, the high selectivity of the CBD reagent for the pedogenic ferrimagnets makes this extraction procedure suitable for determining the causes of the frequency-dependent behaviour of the Argentina loesses at 50–100 K.

2 SAMPLING AND EXPERIMENTS

2.1 Sample description

To determine the relationship between magnetic signals and pedogenic and sedimentological features, part of the samples previously collected and described by Morrás *et al*. (1998a,b) and Nabel *et al.* (1999) were used. The samples pertained to two profiles located at a distance of about 4 km one from the other in the so-called 'Rolling Pampa', a pampean subregion in the of eastern humid Argentina. Table 1 shows the location and site characteristics of these profiles and also of the Spanish soils and the Chinese Central Loess Plateau (CLP) loess/paleosols with which the Argentinian soils are compared in this work. The samples were composite samples (mixtures) of each individual soil horizon.

2.2 Experiments

First, samples were air-dried and were then ground to <2 mm. The particle size distribution was analysed with the pipette method. The organic carbon was measured using dichromate oxidation. The pH

Table 1. Location and site data of the soils considered in this work.

Region	Profile	Location	Mean annual temperature	Mean annual precipitation	Geomorphic position	Parent material	Soil classification*
Undulating Pampa, Argentine							
	CAS	34° 36′ S, 58° 39′ W	16.9 °C	1024 mm	Mid-slope	(Reworked?) loess deposits	Typic Argiudoll
	GAO	34° 38′ S, 58° 37′ W	16.9 °C	1024 mm	Summit	(Reworked?) loess deposits	Vertic Argiudoll
River Guadalquivir Valley, southern Spain (Torrent *et al*. 2010)							
	RB	37° 36′ N, 4° 41′ W	17 °C	580 mm	Mid-slope	Calcarenite	Calcic Haploxeralf
	MO	37° 35′ N, 4° 39′ W	17 °C	580 mm	Mid-slope	Calcarenite	Calcic Haploxeralf
Chinese Loess Plateau (Torrent *et al*. 2007)							
	Paleosols, Luochuan section	35.76 N, 109 °.42′ E	9.2 °C	622 mm	Buried, subhorizontal layers	Quaternary loess units of the Luochuan section	Mostly Calcic Haplustalfs

*According to 'Soil Taxonomy' (Soil Survey Staff 1999).

was determined potentiometrically in 1 : 2.5 soil-water suspensions. The total $CaCO_3$ was estimated by weight loss upon treatment with 6 M HCl.

To isolate the lithogenic contents from the pedogenic contents, 1 g of finely ground (<0.1 mm) parallel samples were treated with 50 ml of the CBD solution according to the method of Mehra & Jackson (1958) except that the suspension was shaken in a reciprocating shaker at 25 °C for 16 h to minimize silicate clay dissolution; the subscript 'post-CBD' is used here for the CBD-treated samples (e.g. '$\chi_{\text{post-CBD}}$').

Total Fe (Fe_t) was determined by treating 100 mg of finely ground sample with 5 ml of 50 per cent HF plus 0.5 ml of 70 per cent $HClO_4$ in a 50-ml Teflon beaker, heating to dryness, moistening the residue with 1 mL of deionized water and 0.2 ml of $HClO_4$, heating again to dryness and dissolving the residue in 6 M HCl. Iron in solution was determined with the *o*-phenanthroline method (Olson & Ellis, 1982) using a measuring wavelength of 508 nm. The ratio between CBD-extractable Fe (Fe_d) and total Fe, that is, Fe_d/Fe_t was used here as an indicator of the relative degree of weathering, as usually done for soils on loess (e.g. Torrent *et al.* 2007). It must be noted that though the absolute values of Fe_t and Fe_d of the studied profiles showed minor differences with those previously obtained by Morrás *et al.* (1998b), the trends were similar in both series of analyses.

For both raw and CBD-treated samples, χ was measured using a Kappa Bridge (Agico, Brno, Czech Republic). The frequency-dependent part of χ was measured using a Bartington Susceptibility Meter at high (4700 Hz) and low (470 Hz) frequency. The difference in magnetic signal between the bulk and the CBD-treated sample, which, as discussed before, can be attributed to the submicron, pedogenic ferrimagnets is denoted by the subscript 'pedo'. For example, $\chi_{\text{pedo}} = \chi - \chi_{\text{post-CBD}}$ and $\chi_{\text{fd,pedo}} = \chi_{\text{fd}} - \chi_{\text{fd,post-CBD}}$.

Low-temperature measurements were conducted using a Quantum Design Magnetic Properties Measurement System (MPMS). The low-temperature dependence of susceptibility ($\chi_{\text{fd}}(T)$, where $\chi_{\text{fd}} = \chi_{1\text{Hz}} - \chi_{10\text{Hz}}$ and T denotes temperature) was determined in this case at dual frequencies (1 and 10 Hz), with the field set at 0.3 mT. Thermal demagnetization of the IRM acquired in 2.5 *T* at 10 K after cooling in a zero field from 300 K was measured from 10 to 300 K. The temperature sweeping rate was 5 K min^{-1}. To determine the exact magnetic carrier of the low-temperature χ_{fd}, low-temperature experiments were also conducted on the magnetic extracts obtained from the sample CAS487 using a high-gradient magnet after the sample was diluted in water.

Magnetic susceptibility of representative samples was measured as a function of temperature using a Kappa Bridge 3 instrument equipped with a CS-3 furnace between room temperature and 700 °C in an argon atmosphere to prevent oxidation (flux rate: 100 ml min^{-1}). To determine the possible mineral transformation at high temperatures, stepwise $\chi(T)$ curves were also measured. The maximum treatment temperature for each run was named $T_{\max}$. In addition, magnetization curves in a field of 300 mT were measured as a function of temperature for stepwise increasing maximum temperatures of 300, 500 and 600 °C.

The concentrations of goethite and hematite were estimated by diffuse reflectance (DR) spectroscopy as described in more detail by Torrent *et al*. (2007). DR spectra were recorded at a scan rate of 30 nm min^{-1} from 380 to 710 nm in 0.5 nm steps, using a Varian Cary 1E spectrophotometer equipped with a $BaSO_4$–coated integrating sphere 73 mm in diameter (Varian Inc., Palo Alto, CA).

3 RESULTS

Table 2 shows selected physical, chemical and mineralogical properties of the soils. The upper part of the argillic horizon (Bt1) of both profiles is rich in clay (37 per cent in CAS and 54 per cent in GAO) and exhibits the highest concentration in free Fe oxides (as estimated by Fe_d). The (hematite)/(hematite + goethite) [Hm/(Hm+Gt)] ratio ranges between 0.44 and 0.63 in the CAS and between 0.56 and 0.65 for the GAO profile with no clear upward trend in either profile. A clearer upward trend is seen on the degree of weathering of Fe-bearing minerals as evaluated from the Fe_d/Fe_t ratio, which goes from 0.089 (in Ckm) to 0.217 (in A) in the CAS profile and from 0.064 (in Ck1) to 0.178 (in A/B) in the GAO profile; however, the concentration in pedogenic ferrimagnets, as represented by χ_{pedo}, shows only a weak upward trend (Table 3).

According to the Fe_d/F_t ratio, the CLP paleosols are slightly more weathered (Fe_d/F_t goes from ~0.23 in unweathered loess to ~0.37 in the most developed paleosols) relative to the Pampean soils and show a marked upward increase in the [Hm/(Hm+Gt)] ratio (from about ~0.3 in the parent loesses to ~0.55 in the most strongly weathered paleosols (Torrent *et al*. 2007); this suggests that pedogenesis favours hematite over goethite. The Spanish soils

Table 2. Selected physical, chemical and mineralogical properties of the CAS and GAO soil samples.*

Horizon	Depth (cm)	Sample code	Munsell colour	Clay ($g\ kg^{-1}$)	Sand ($g\ kg^{-1}$)	pH (water)	$CaCO_3$ ($g\ kg^{-1}$)	Organic matter ($g\ kg^{-1}$)	Fe_t ($g\ kg^{-1}$)	Fe_d ($g\ kg^{-1}$)	Fe_d/Fe_t	Hm/(Hm+Gt)	Gt ($g\ kg^{-1}$)	Hm ($g\ kg^{-1}$)
CAS (Typic Argiudoll)														
A	0–25	CAS-486	7.5 YR 4/3	290	155	7.3		17.4	25.2	5.45	0.217	0.44	3.8	3.0
Bt1	25–55	CAS-487		368	131	6.9		7.4	34.1	5.58	0.164	0.58	3.2	4.4
Bt2	55–111	CAS-488	7.5 YR 5.3	420	105	6.8		3.7	37.2	3.83	0.103	0.62	1.9	3.2
BC	111–131	CAS-489		322	130	7.0		1.6	33.4	5.62	0.168	0.59	3.2	4.6
2Ckm	131–150	CAS-490	7.5 YR 6.3	201	388	8.0	18	1.2	28.6	2.54	0.089	0.63	1.4	2.3
GAO (Vertic Argiudoll)														
A/B	0–20	GAO-625		296	141	7.5		9.1	24.8	4.41	0.178	0.56	2.0	2.6
Bt1	20–60	GAO-626	7.5 YR 3/3	539	75	7.2		5.3	34.3	4.87	0.142	0.57	2.5	3.3
Bt2	60–100	GAO-627	7.5 YR 4/4	558	75	7.1		3.8	38.0	4.20	0.111	0.65	2.0	3.7
BCk	100–150	GAO-628	7.5 YR 5/4	323	97	7.7	156	3.5	30.5	2.12	0.070	0.62	1.1	1.7
Ck1	150–250	GAO-629	7.5 YR 5/4	395	36	7.7	45	1.4	36.9	2.37	0.064	0.58	1.4	1.9

*Munsell colour for dry ground samples. The subscripts d and t for Fe indicate citrate/bicarbonate/dithionite (CBD)-soluble and total, respectively. Hm and Gt indicate hematite and goethite, respectively.

Table 3. Summary of the magnetic properties of the CAS and GAO samples.*

Horizon	Depth (cm)	Sample	χ_{bulk}	$\chi_{fd,bulk}$ per cent	$\chi_{lithogenic}$	χ_{pedo}	$\chi_{fd,bulk}$	$\chi_{fd,lithogenic}$	$\chi_{fd,pedo}$
CAS (Typic Argiudoll)									
A	0–25	CAS-486	28.2	5	15.2	13.0	1.41	0.15	1.26
Bt1	25–55	CAS-487	27.9	4	14.9	13.0	1.12	0.15	0.97
Bt2	55–111	CAS-488	23.5	4	13.3	10.2	0.94	0	0.94
BC	111–131	CAS-489	23.5	3	15.2	8.3	0.71	0.15	0.55
2Ckm	131–150	CAS-490	22.6	5	13	9.6	1.13	0	1.13
GAO (Vertic Argiudoll)									
A/B	0–20	GAO-625	9.6	4	6.7	2.9	0.35	0.07	0.28
Bt1	20–60	GAO-626	9.4	4	6.1	3.3	0.38	0.06	0.32
Bt2	60–100	GAO-627	15.5	4	8.1	7.4	0.62	0.08	0.54
BCk	100–150	GAO-628	7.9	4	4.5	3.4	0.32	0.05	0.27
Ck1	150–250	GAO-629	5.3	5	3.4	1.9	0.27	0.03	0.23

*The unit of χ and χ_{fd} is $10^{-7}\ m^3\ kg^{-1}$. The subscript bulk, lithogenic and pedo indicate the contributions from the bulk sample, the post-CBD residues and the CBD-soluble components, respectively.

are the most strongly weathered ones (Fe_d/F_t goes from ~0.25 in unweathered calcarenite to ~0.50 in the upper soil horizons) and exhibit the highest values for the [Hm/(Hm+Gt)] ratio (up to ~0.7) (Torrent *et al*. 2010). These differences in the [Hm/(Hm+Gt)] ratio could be the result of differences in climate and age among the three groups of soils.

The $\chi(T)$ curves for representative bulk samples (Fig. 1) exhibit a sharp decrease in χ from 5 to 50 K, which can be attributed to the paramagnetic components. The slight kinks at about 120 K (corresponding to the Verwey transition of magnetite) for samples CAS488 and GAO627 indicate the presence of magnetite. The increase in χ with increasing temperature below about 250 °C is likely due to the gradual unblocking of SSD particles or the release of stress upon heating. The Curie temperatures of ~580 °C further indicate the presence of magnetite. It must be noted that the $\chi(T)$ curves for these samples share great similarities except that the relative paramagnetic contributions are higher for the GAO than for the CAS series because the latter have enhanced magnetic properties, which are carried mostly by the ferrimagnetic components.

Stepwise $\chi(T)$ curves for representative samples are shown in Fig. 2. The raw and the CBD-treated samples exhibit different thermal behaviour. The χ values gradually increase up to ~200°C mostly due to the gradual unblocking of SD particles. The slight increase in the room-temperature χ for the 300 °C run could be due to the partial dehydration of goethite to hematite. For the raw sample CAS486, mineral transformation occurred even for the 300 °C run. So, the cooling curve exhibits higher χ values at room temperature than the heating curve (Fig. 2a). For $T_{max} = 500\,°C$, and between ~250 and 500 °C, the lower values for the cooling curve mostly indicate the transformation of maghemite to weakly magnetic hematite (Fig. 2b). However, it is hard to detect the newly formed hematite using $\chi(T)$ curves because the magnetization of hematite is about two orders in magnitude lower than that of magnetite.

When T_{max} reaches 600 °C, the reversible $\chi(T)$ curves indicate that mineral transformation processes are nearly completed. The Curie temperatures of 580 °C indicate that magnetite constitutes the most stable phase in the raw sample. In addition, there also exists a susceptibility kink around 300 °C, which indicates either the T_c of titanomagnetite or effects from the GSD. For the CBD-treated sample, the 300 °C treatment caused a conspicuous mineral transformation (Fig. 2d). In contrast, for the 400 °C run (Fig. 2e), the nearly reversible feature indicates that the thermally unstable phase maghemite was mostly removed by the CBD treatment. After the 600 °C run, the cooling curve (Fig. 2f) resembles that of the raw sample (Fig. 2c).

The raw sample GAO627 exhibits at lower temperatures ($T_{max} <$ 500 °C) a thermal behaviour similar to that of the raw sample CAS486 (Figs 2a,b,g,h), but at more elevated temperatures, its cooling curve lies markedly below its warming one (Fig. 2i), which points to a mineral transformation. In contrast, the corresponding CBD-treated sample shows nearly reversible features for all runs (Figs 2j–l). The unique T_c of ~580 °C indicates that only magnetite is dominant in the sample.

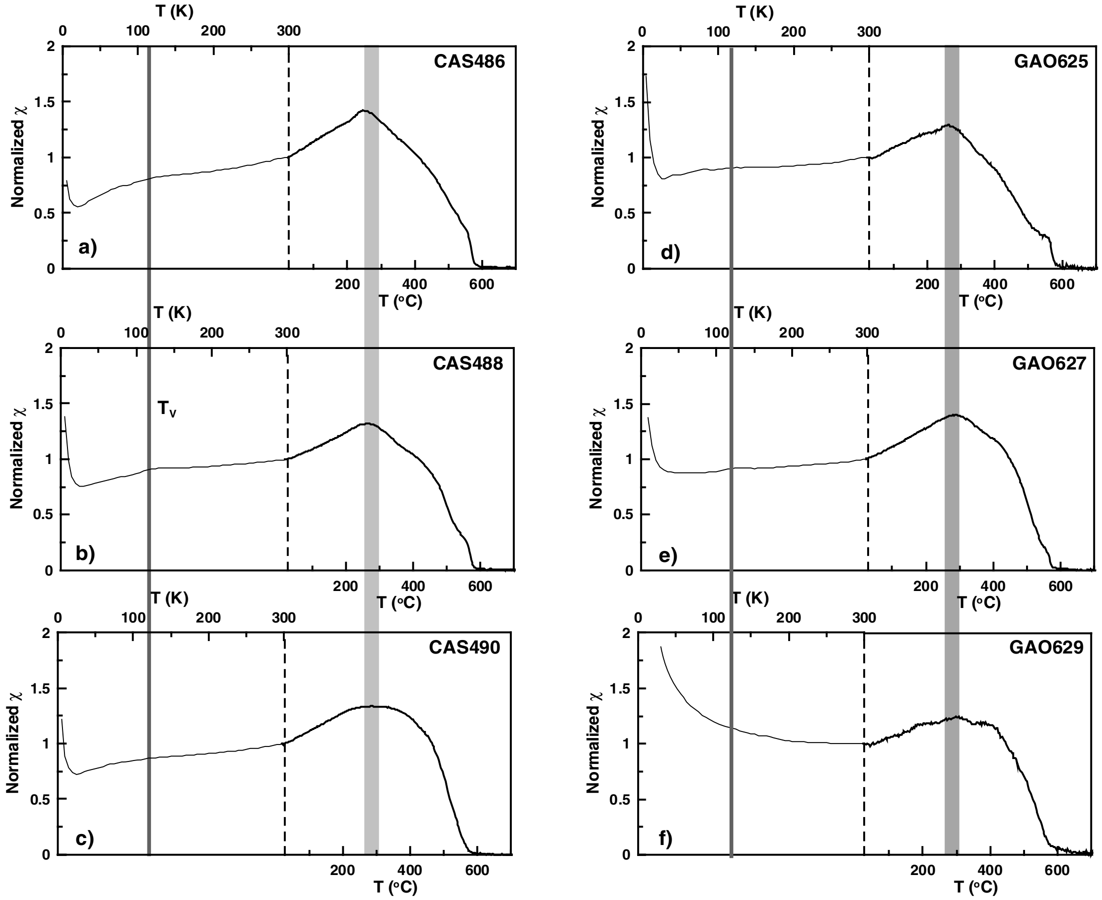

Figure 1. Composite temperature-dependent magnetic susceptibility (χ–T) curves for representative samples from the CAS (a)–(c) and GAO profiles (d)–(f). The low-temperature (<300 K) and high-temperature (>300 K) curves are measured by the MPMS and Kappa Bridge, respectively. The thin and thick grey lines mark the Verwey transition (120 K) and the temperature for the χ peak, respectively. The dashed line indicates the room temperature. The curves were normalized by the room-temperature values.

The stepwise J(T) curves (Fig. 3a) show reversible features when $T_{max} = 300\,^{\circ}$C, which indicates no detectable mineral transformation occurred at this stage. When $T_{max} = 500\,^{\circ}$C, the heating and cooling curves differed (Fig. 3b). The cooling curve is lower than the heating curve at the room temperature, which indicates that some strongly magnetic minerals have been transformed into weakly magnetic phases. After the 600 °C run, the room-temperature J is about 80 per cent of the initial value (Fig. 3c). Except for the T_c of 580 °C, the J(T) curves are rather smooth. This strongly indicates that the 300 °C susceptibility kinks on the $\chi(T)$ curves are caused by effects from the GSD. Therefore, magnetite is the dominant phase. Maghemite could also exist reflected by the thermally unstable behaviour above 300 °C.

The most notable feature of $\chi_{fd}(T)$ is a pronounced peak between 50 and 100 K. Both the CAS and the GAO measurements can be considered as the superposition of this peak and a 'background' that is weakly dependent on temperature. To investigate the origin of this feature in the bulk sample, we measured $\chi_{fd}(T)$ on the same sample after CBD treatment, which is known to dissolve the finer fraction of magnetic minerals. The CBD treatment removed the 'background', leaving intact the very uniform $\chi_{fd}(T)$ peak between 50 and 100 K (Fig. 4). Therefore, we interpret the 'background' as the susceptibility of CBD-extractable magnetic particles, which has been calculated by subtracting $\chi_{fd}(T)$ after CBD treatment from $\chi_{fd}(T)$ of the bulk (Figs 4e and f). On the other hand, the $\chi_{fd}(T)$ peak is an inherent feature of the sedimentary parent material rather than of the submicron ferrimagnetic minerals generated during pedogenesis.

The thermal demagnetization of the SIRM curves acquired in 2.5 T at 10 K for raw samples is shown in Fig. 5. Overall, the remanence was gradually demagnetized upon warming (Figs 5a and b). The room-temperature remanences are only about 20 per cent of the initial values at 10 K, which indicates the presence of SP particles. Detectable remanence kinks at ~120 K for some samples indicate the Verwey transition for magnetite. The smeared Verwey transition indicates that magnetite might have been partially oxidized (Özdemir *et al*. 1993; van Velzen & Dekkers 1999).

The low-temperature χ and χ_{fd} curves for the magnetic extracts of the sample CAS487 are shown in Fig. 6. The kink around 120 K on the $\chi(T)$ curves indicate that magnetite is present. The $\chi_{fd}(T)$ for the extract also exhibits a dominant peak around 50 K, which resembles that of the bulk sample (Fig. 5).

4 DISCUSSION

4.1 Origin of the χ_{fd} peak at 50 K

The χ_{fd} peak at about 50 K in some Pampean paleosols and modern soils has been attributed to the presence of extremely-fined grained magnetic particles of pedogenic origin (Orgeira *et al*. 2003; Vasquez *et al*. 2009). Luis *et al*. (1999) have studied the χ_{fd} curve

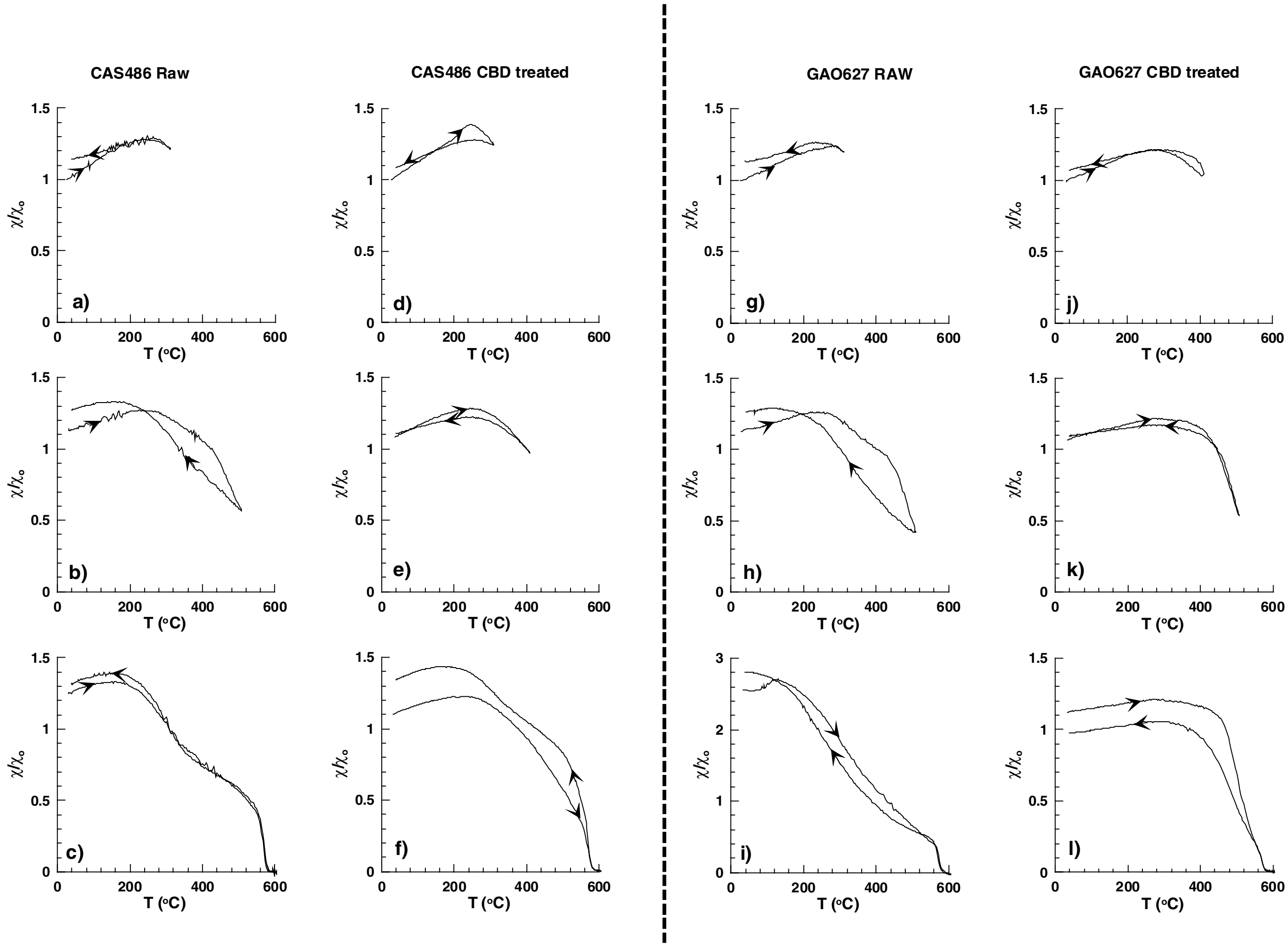

Figure 2. Stepwise $\chi(T)$ curves for the sample CAS486 (left column) and GAO627 (right column). (a)–(c) and (g)–(i) raw sample, (d)–(f) and (j)–(l) the post-CBD sample. Arrows indicate the heating and cooling processes.

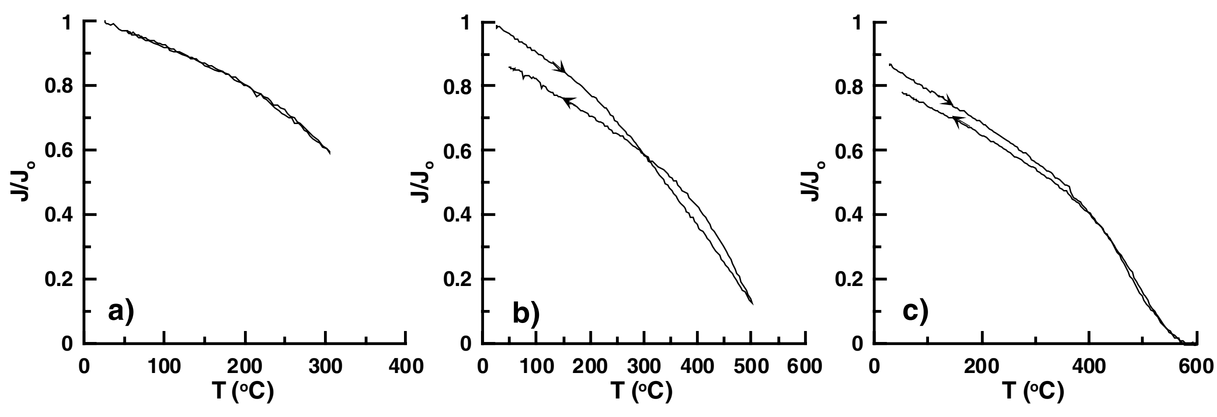

Figure 3. Stepwise J(T) curves for the sample CAS486 (CBD treated). Arrows indicate the warming/cooling processes.

of nano-sized ferritin particles with a well-controlled GSD. If the $\chi_{\rm fd}$ peak below the Verwey transition in our samples is indeed caused by fine-grained particles, the GSD of these particles will be extremely narrow. Such exceptionally well-controlled magnetic particles should be formed in a rather strict environment and have not been reported in other regions.

Our results show that after the CBD treatment, these peaks are carried dominantly by the residuals. It is well-known that the CBD procedure (Mehra & Jackson 1958) preferentially dissolves the pedogenic Fe oxides of submicron particle size, but has little effect on lithogenic magnetite with size above 1 μm (Hunt *et al*. 1995). Although small-sized magnetite (< 1 μm) can also be partially dissolved, the lithogenic ferrimagnets lie mostly above this grain size threshold (Hunt *et al*. 1995) and thus the CBD method is useful for separating the lithogenic from the pedogenic components. Typically, the CBD-treated residue shows grey colours and the absence of the typical bands for Fe oxides in the diffuse reflectance spectrum. Therefore, it is confidently concluded that the

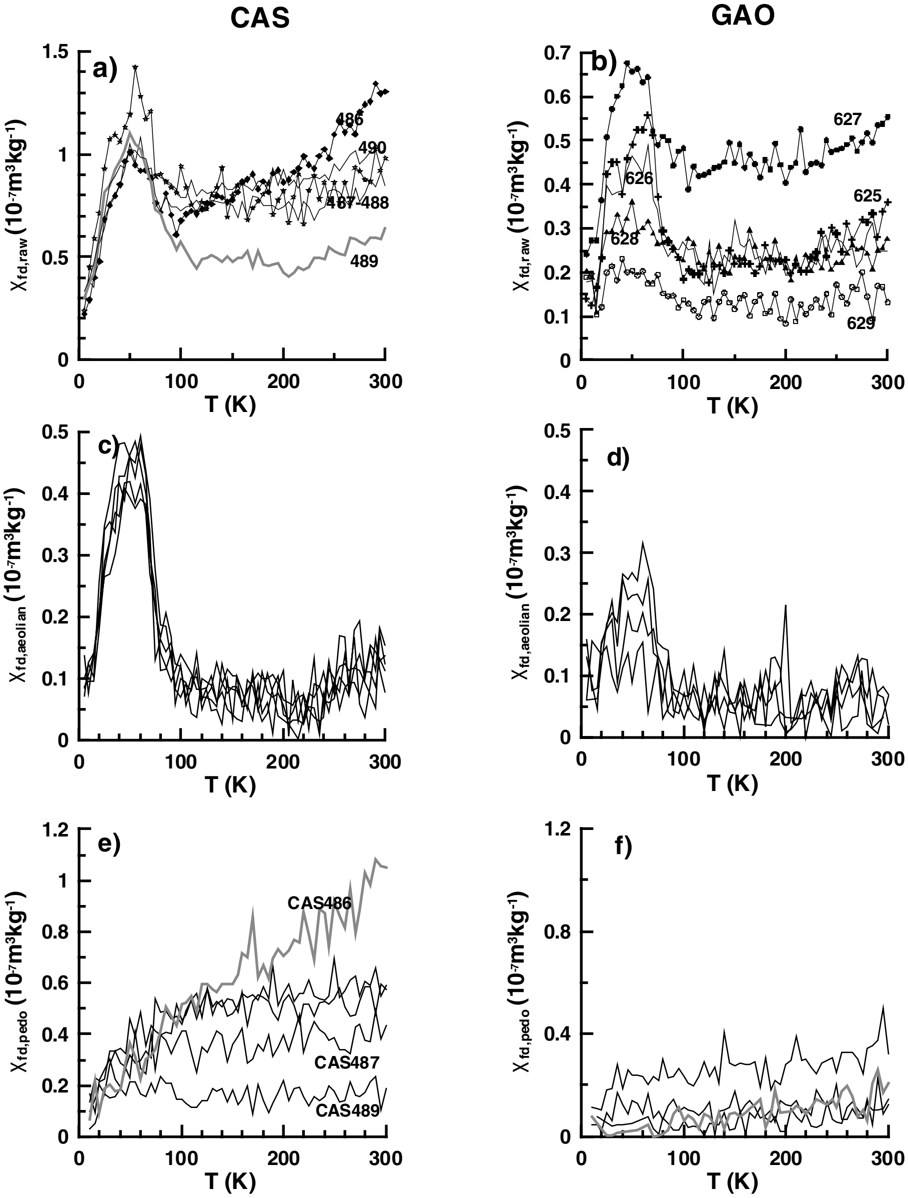

Figure 4. Low-temperature χ_{fd}–T curves for samples from the CAS (left column) and GAO (right column) profiles. (a), (b) bulk sample, (c), (d) the lithogenic inputs (the post-CBD residues) and (e), (f) the pedogenic components (the CBD-soluble components).

magnetic behaviour (specifically the 50 K χ_{fd} peak) of the residues after the CBD treatment pertains to iron oxides of lithogenic origin—and is thus independent of pedogenic magnetic mineral neoformation.

The magnitude of the 50 K χ_{fd} peak differs between profiles. This suggests that the concentration of the magnetic material responsible for that peak differs significantly between the two profiles probably because (i) the proportion of the depositional coarse fraction (sand + silt, i.e. the non-clay fraction) are rather different between the two profiles (Table 2) and mainly, (ii) the two soils differ mineralogically. Morrás *et al.* (1998a,b) and Nabel *et al*. (1999) found in this respect that the GAO and CAS soils clearly differed in their geochemical and mineralogical composition: several major (Fe, Ti, Na, K) and minor elements (Mn, Cr, Zn) are in different proportion in both profiles; the major and trace element content of both profiles also differ from the contents reported for the Chinese loess (Morrás *et al*. 1998b). Clay fraction in CAS is dominantly illitic while clay in GAO is dominantly smectitic; some differences in the silt and sand of two profiles were also observed through XRD and SEM analyses, particularly concerning the volcanic glass content. More precise information on sand mineralogy of both profiles is here shown in Table 4: the contents of quartz, feldspars and volcanic glass and their relationships in the light sand fraction confirm previous results and point to some differences in the source and transport of sediments of these profiles (Morrás 2003).

It is noted that such a $\chi_{fd}(T)$ peak is absent in the Chinese or Spanish soils (Torrent *et al*. 2007). A possible reason is that the lithogenic components for the Chinese or Spanish soils have a rather weak magnetism and the information has been highly masked by the strong magnetic background due to the neoformation of pedogenic particles. On the contrary, volcaniclastic inputs give distinct magnetic properties to the soil parent materials in Argentina. Further studies on parent material are essential to distinguish the exact mechanism.

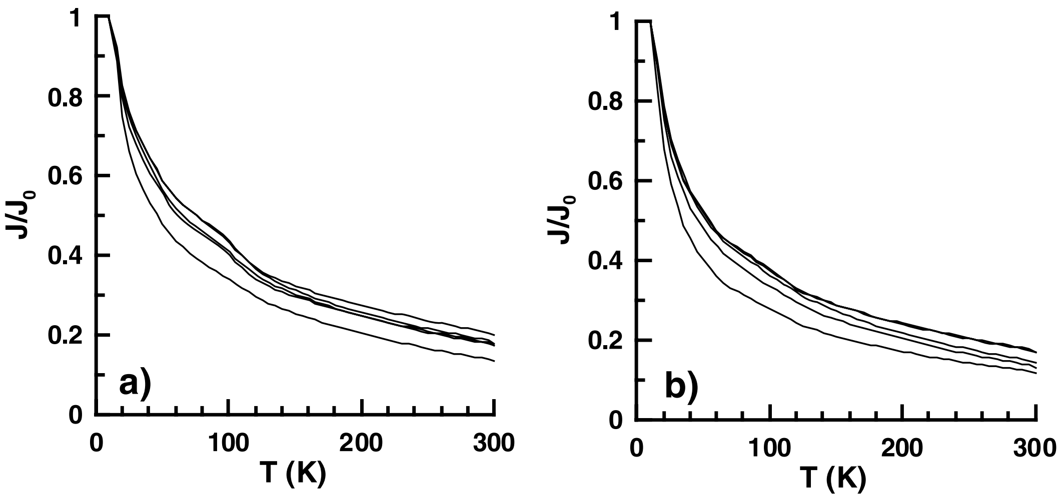

Figure 5. Low-temperature thermal demagnetization of SIRM acquired in 2.5 *T* at 10 K. (a) and (b) are for the CAS and GAO raw samples, respectively. The small kink near 120 K indicates Verwey transition if magnetite.

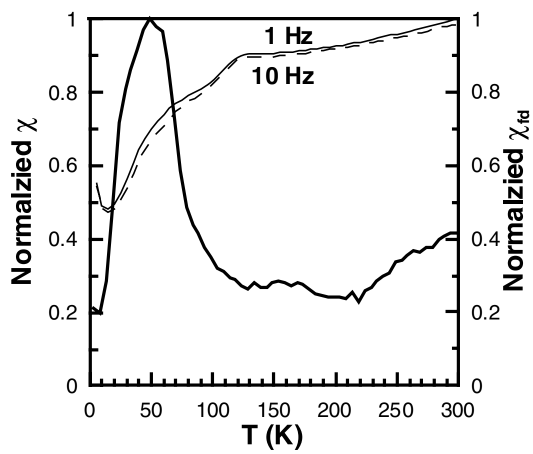

Figure 6. The low-temperature behaviour of the magnetic extract for the sample CAS487. The χ curves were measured at dual frequencies of 1 and 10 Hz, respectively. The thick line indicates the χ_{fd} normalized by the maximum at ~50 K.

4.2 Mechanism of the χ_{fd} peak at 50 K

The frequency-dependence of magnetic susceptibility behaviour of the lithogenic fraction below the Verwey transition can be caused most probably by two mechanisms: superparamagnetism and the relaxation of domain walls associated with the coarse-grained PSD/MD (pseudo-single domain/multi-domain) magnetic particles (magnetite or titanomagnetite) (Simša *et al.* 1985; Radhakrishnamurthy & Likhite, 1993; Moskowitz *et al.* 1998; Skumryev *et al.* 1999; Kosterov 2003; Lagroix *et al*. 2004).

Because the 50 K χ_{fd} peak is rather resistant to the CBD treatment, the corresponding carriers cannot be isolated fine-grained particles. Considering the volcaniclastic origin of most pampean loess deposits, Bidegain *et al.* (2005) studied the magnetic properties of an ash layer occurring in a loess-paleosol sequence in Mar del Plata. They found that the magnetic susceptibility and the corresponding χ_{fd} per cent are both a function of the grain size fraction of the raw ash material. The <63 μm fraction is the most magnetic, but the 80–140 μm fraction has the maximum χ_{fd} per cent values. On the basis of the observation of Teruggi (1957) that pyroxene grains in the sand fraction of pampean loess always contain opaque minerals, Bidegain *et al*. (2005) further suggested that these inclusions could be potential sources for the frequency-dependent behaviour if the grain sizes of these inclusions extends down to the submicrometer range. However, as discussed above, it is rather unrealistic for the inclusions to have such a well-defined narrow GSD.

Alternatively, the 50 K χ_{fd} peak is a common phenomenon associated with the relaxation of the domain walls of the coarse-grained magnetic particles. The domain wall for multidomain material is not fixed and the domain wall displacement (DWD) associated

Table 4. Mineralogical composition of the light sand fraction of CAS and GAO profiles.*

	Quartz (Q) per cent	Feldspars (F) per cent	Volcanic glass (V) per cent	Volcanic fragments per cent	Q/F	(Q/F+V).100
CAS-486	5	63	23	9	0.08	5.8
487	10	67	12	11	0.15	12.6
488	10	70	4	15	0.14	13.5
489	4	40	53	3	0.10	4.3
490	8	70	10	10	0.11	10.0
GAO-625	15	66	6	13	0.23	20.8
626	16	62	4	16	0.26	24.2
627	16	64	2	17	0.25	24.2
628	17	66	<1	16	0.26	25.7
629	9	69	1	21	0.13	12.8

*Feldspars include potassic feldspars as well as plagioclases. The (Q/F+V)100 index, according to Morrás & Delaune (1985) and Morrás (2003). Absolute values and relationships show differences between both profiles.

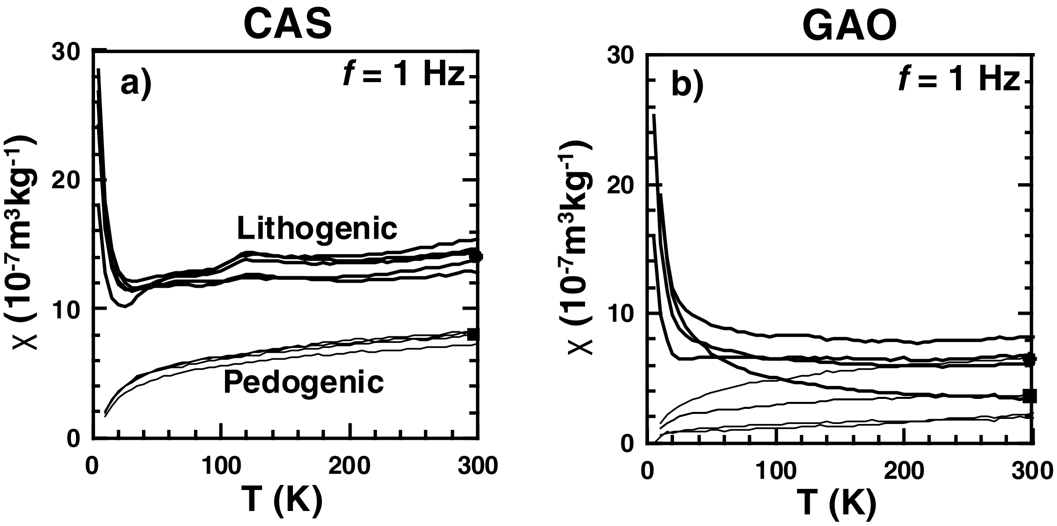

Figure 7. Comparison of the low-temperature χ–T curves for the lithogenic and pedogenic components of the CAS (a) and GAO (b) series. The measurement frequency is 1 Hz. The solid circle and rectangle indicate the average room-temperature χ values for the lithogenic and pedogenic components, respectively. The thick and thin curves indicate the lithogenic and pedogenic components, respectively.

with the corresponding relaxation process will interact with the structural domains (Balanda *et al.* 2005). However, at temperatures <60 K, the DWD will be confined by the ionic order within walls due to magnetoelectric effects (the rotation of magnetization of magnetite will induce an electric field and vice versa). With further increasing temperatures, the magnetoelectric effects gradually disappear. Therefore, the magnetoelectric effects can be viewed as friction on the domain wall, which is further affected by the thermal agitation. For our samples, titanomagnetite can be excluded because of the lack of the corresponding Curie temperature. Thus, a much more reasonable explanation of the frequency-dependence χ below the Verwey transition is the coarse-grained magnetite (e.g. Skumryev *et al.* 1999; Balanda *et al.* 2005), which is always characterized by narrow peaks below the Verwey transition. The characteristic temperature of such peaks is highly sensitive to the degree of non-stoichiometry (e.g. substitutions and vacancies) (Balanda *et al*. 2005). This could also explain why the Verwey transition is depressed for multidomain magnetite in our samples (Fig. 5).

4.3 Geological and pedological implications

Fig. 7 compares the low temperature variations in $\chi_{\rm lithogenic}$ (i.e. $\chi_{\rm post-CBD}$) and pedogenic (i.e. $\chi_{\rm pedo}$) χ values for the CAS and GAO profiles. At room temperature, in the case of the CAS profile, the average χ values for the aeolian and pedogenic components are about 14.0×10^{-7} m^3 kg^{-1} and 8.0×10^{-7} m^3 kg^{-1}, respectively. For the GAO profile, the corresponding values are about 6×10^{-7} m^3 kg^{-1} and 4×10^{-7} m^3 kg^{-1}, respectively. It is interesting to note that the difference between the lithogenic and pedogenic contributions to χ values are less marked in the GAO than in the CAS samples. This appears consistent with the geochemical and mineralogical differences and the lower content of volcaniclastic minerals in the GAO profile compared to CAS profile as was indicated by Morrás *et al*. (1998a,b) and Nabel *et al*. (1999) and it is here confirmed by the mineralogical analysis of the sand fraction (Table 4). These results also confirm the interpretations of Morrás *et al.* (2004a,b) studying a considerable number of modern soil profiles in the same area of CAS and GAO profiles, about the dominant influence of lithogenic components on their bulk magnetic susceptibility.

Unlike the soils from the CLP and Spain, where the lithogenic inputs or the parent calcarenite are relatively uniform with low χ values, the $\chi_{\rm lithogenic}$ for the Argentina soils accounts for more than 60 per cent of the total signal. Therefore, variations in $\chi_{\rm lithogenic}$ can certainly distort or even suppress the pedogenic signals. By removing effects from $\chi_{\rm lithogenic}$, $\chi_{\rm fd,pedo}$ per cent for pure pedogenic particles is much enhanced.

5 CONCLUSIONS

Using the CBD treatment, the magnetic properties of the bulk samples are decomposed into two parts of different origin: the CBD-soluble fraction of pedogenic origin and the residues of lithogenic origin. The 50 K $\chi_{\rm fd}$ peak is an inherent feature of the sedimentary material and thus independent of pedogenesis. One probable mechanism for such peaks is the relaxation of domain walls associated with the coarse-grained PSD/MD magnetic particles of lithogenic origin. Because the magnetic susceptibility carried by the lithogenic components contributes significantly to the bulk values, we propose that the CBD-soluble magnetic signals could be more appropriate proxies to trace the long-term paleoenvironmental variations in this region.

ACKNOWLEDGMENTS

This study was supported by National Nature Science Foundation of China (NSFC) 40974036, 40821091 and the CAS/SAFEA International Partnership Program for Creative Research Teams and by the Chinese Academy of Sciences. Q. Liu further thanks ‘100 Talent Program of the Chinese Academy of Sciences’. Y.L. Su further thanks supports from NSFC 40874033. The contribution of J. Torrent was partly supported by Spain’s Ministerio de Educación y Ciencia, Project AGL2006-10927-CO3-C02 and the European Regional Development Fund. The work of H. Morrás was supported by INTA-AERN 5653 Project and other INTA funds. We thank two anonymous reviews, Dr. C. Geiss and the editor (Prof. E. Appel) for their instructive comments to improve the quality of this manuscript.

REFERENCES

Balanda, M., Wiechec, A., Kim, D., Kakol, Z., Kozlowski, A., Niedziela, P., Sabol, J., Tarnawski, Z. & Honig, J.M., 2005. Magnetic AC susceptibility of stoichiometric and low zinc doped magnetite single crystals, *Eur. Phys. J. B,* **43,** 201–212.

Bartel, A., 2009. Caracterización magnética de una climosecuencia de suelos entre el sureste de la Provincia de La Pampa y el Litoral Atlántico, *PhD thesis*, Departamento de Geología, Universidad Nacional del Sur, Bahía Blanca, Argentina, 259 p.

Begét, J., 1996. Tephrochronolgy and paleoclimatology of the last interglacial cycle recorded in Alaska loess deposits, *Quat. Int.,* **34–36,** 121–126.

Begét, J. & Hawkins, D., 1989. Influence of orbital parameters on Pleistocene loess deposition in central Alaska, *Nature,* **337,** 151–153.

Begét, J., Stone, D. & Hawkins, D., 1990. Paleoclimate forcing of magnetic susceptibility variations in Alaskan loess, *Geology,* **18,** 40–43.

Bidegain, J.C. & Rico, Y., 2004. Mineralogía magnética y registros de susceptibilidad en sedimentos cuaternarios de polaridad normal (Brunhes) y reversa (Matuyama) de la cantera de Juárez, provincia de Buenos Aires, *Rev. Asoc. Geol. Argent.,* **59,** 451–461.

Bidegain, J.C., van Velzen A. & Rico, Y., 2001. Parámetros magnéticos en una secuencia de loess y paleosuelos del Cenozoico tardío en la cantera de Gorina, La Plata: su relevancia en el estudio de los cambios paleoclimáticos y paleoambientales, *Rev. Asoc. Geol. Argent.,* **56,** 503–516.

Bidegain, J.C., Evans, M.E. & van Velzen, A.J., 2005. A magnetoclimatological investigation of Pampean loess, Argentina, *Geophys. J. Int.,* **160,** 55–62.

Bidegain, J.C., Rico, Y., Bartel, A., Chaparro, M. & Jurado, S., 2009. Magnetic parameters reflecting pedogenesis in Pleistocene loess deposits of Argentina, *Quat. Int.,* **209,** 175–186

Bloemendal, J. & Liu, X.M., 2005. Rock magnetism and geochemistryof two Plio-Pleistocene Chinese loess-palaeosol sequences—Implicationsfor quantitative palaeoprecipitation reconstruction, *Palaeogeogr. Palaeoclimatol. Palaeoecol.,* **226,** 149–166.

Bugglea, B., Glaser, B., Zöller, L., Hambach, U., Marković, S., Glaser, I. & Gerasimenko, N., 2008. Geochemical characterization and origin of Southeastern and Eastern European loesses (Serbia, Romania, Ukraine), *Quat. Sci. Rev.,* **27,** 1058–1075.

Castiglioni, M., Morrás, H., Santanatoglia, O., Altinier, M.V. & Tessier, D., 2007. Movimiento del agua en Argiudoles de la Pampa Ondulada con diferente mineralogía de arcillas, *Ciencia del Suelo,* **25,** 109–122.

Chen, T.H., Xu, H.F., Xie, Q.Q., Chen, J., Ji, J.F. & Lu, H.Y., 2005. Characteristics and genesis of maghemite in Chinese loess and paleosols: mechanism for magnetic susceptibility enhancement in paleosols, *Earth planet. Sci. Lett.,* **240,** 790–802.

Chlachula, J., Rutter, N.W. & Evans, M.E., 1997. A late Quaternary loess-Paleosol record at Kurtak, southern Siberia, *Can. J. Earth Sci.,* **34,** 679–686.

Chlachula, J., Evans, M.E. & Rutter, W., 1998. A magnetic investigation of a late Quaternary loess/palaeosol record in Siberia, *Geophys. J. Int.,* **132,** 128–132.

Dearing, J.A., Dann, R.J.L., Hay, K., Lees, J.A., Loveland, P.J., Maher, B.A. & O'Grady, K., 1996. Frequency-dependent susceptibility measurements of environmental materials, *Geophys. J. Int.,* **124,** 228–240.

Deng, C.L., Vidic, N.J., Verosub, K.L., Singer, M.J., Liu, Q.S., Shaw, J. & Zhu, R.X., 2005. Mineral magnetic variation of the Jiaodao Chinese loess/paleosol sequence and its bearing on long-term climatic variability, *J. geophys. Res.,* **110**(B3), B03103, doi:10.1029/2004JB003451.

Ding, Z.L., Derbyshire, E., Yang, S.L., Yu, Z.W., Xiong, S.F. & Liu, T.S., 2002. Stacked 2.6-Ma grain size record from the Chinese loess based on five sections and correlation with the deep-sea d18O record, *Paleoceanography,* **17,** 1033, doi:10.1029/2001PA000725.

Etchichury, M. & Tofalo, R., 2004. Mineralogía de arenas y limos en suelos, sedimentos fluviales y eólicos actuales del sector austral de la cuenca Chacoparanense. Regionalización y áreas de aporte, *Rev. Asoc. Geol. Argent.,* **59,** 317–329.

Evans, M.E., Rutter, N.W., Catto, N., Chlachula, J. & Nyvlt, D., 2003. Magnetoclimatology: teleconnection between the Siberian loess record and North Atlantic Heinrich events, *Geology,* **31,** 537–540.

Geiss, C.E. & Zanner, C.W., 2006. How abundant is pedogenic magnetite? Abundance and grain size estimates forloessic soils based on rock magnetic analyses, *J. geophys. Res.,* **111,** B12S21, doi:10.1029/2006JB004564.

Heller, F. & Liu, T.S., 1984. Magnetism of Chinese loess deposits, *Geophys. J. R. Astron. Soc.,* **77,** 125–141.

Heller, F. & Liu, T.S., 1986. Palaeoclimatic and sedimentary history from magnetic susceptibility of loess in China, *Geophys. Res. Lett.,* **13,** 1169–1172.

Hunt, C.P., Singer, M.J., Kletetschka, G., Tenpas, J. & Verosub, K.L., 1995. Effect of citrate-bicarbonate-dithionite treatment on fine-grained magnetite and maghemite, *Earth planet. Sci. Lett.,* **130,** 87–94.

Kosterov, A., 2003. Low-temperature magnetization and AC susceptibility of magnetite: effect of thermomagnetic history, *Geophys. J. Int.,* **154,** 58–71.

Kravchinsky, V., Zykina, S. & Zykin, V.S., 2008. Magnetic indicator of global paleoclimate cycles in Siberian loess-paleosol sequences, *Earth planet. Sci. Lett.,* **265,** 498–514.

Kukla, G.J., Heller, F., Liu, X.M., Xu, T.C., Liu, T.S. & An, Z.S., 1988. Pleistocene climates in China dated by magnetic susceptibility, *Geology,* **16,** 811–814.

Lagroix, F. & Banerjee, S.K., 2004a. The regional and temporal significance of primary aeolian magneticfabrics preserved in Alaskan loess, *Earth planet. Sci. Lett.,* **225,** 379–395.

Lagroix, F. & Banerjee, S.K., 2004b. Cryptic post-depositional reworking in aeolian sediments revealedby the anisotropy of magnetic susceptibility, *Earth planet. Sci. Lett.,* **224,** 453–459.

Lagroix, F., Banerjee, S.K. & Jackson, M.J., 2004. Magnetic properties of the Old Crow tephra: identification of a complex iron titanium oxide mineralogy, *J. geophys. Res.,* **109,** B01104, doi:10.1029/2003JB002678.

Liu, T.S., 1985. *Loess and the Environment,* p. 251, China Ocean Press, Beijing.

Liu, T.S. & Ding, Z.L., 1998. Chinese loess and the paleomonsoon, *Ann. Rev. Earth Planet. Sci.,* **26,** 111–145.

Liu, Q.S., Torrent, J., Maher, B.A., Yu, Y.J., Deng, C.L., Zhu, R.X. & Zhao, X.X., 2005. Quantifying grain size distribution of pedogenic magnetic particles in Chinese loess and its significance for pedogenesis, *J. geophys. Res.,* **110,** B11102, doi:10.1029/2005JB003726.

Luis, F., del Barco, E., Hernández, J.M., Remiro, E. & Bartolomé, J., 1999. Resonant spin tunneling in small antiferromagnetic particles, *Phys. Rev. B,* **59,** 11837–11846.

Maher, B.A., 1998. Magnetic properties of modern soils and Quaternary loessic paleosols: paleoclimatic implications, *Palaeogeogr. Paaleoclimatol. Palaeoecol.,* **137,** 25–54.

Mehra, O.P. & Jackson, M.L., 1958. Iron oxide removal from soils and clays by a dithionite−citrate system buffered with sodium bicarbonate, *Clays Clay Miner.,* **7,** 317–327.

Morrás, H., 1999. Geochemical differentiation of Quaternary sediments from the Pampean region based on soils phosphorous contents as detected in the early 20th century, *Quat. Int.,* **62,** 57–67.

Morrás, H., 2003. Distribución y origen de sedimentos superficiales de la Pampa Norte en base a la mineralogía de arenas. Resultados preliminaries, *Rev. Asoc. Argent. Sediment.,* **10,** 53–64.

Morrás, H. & Cruzate, G., 2002. Origen y distribución del potasio en suelos de la región Chaco-pampeana, in *El potasio en sistemas agrícolas argentinos*, pp. 35–47, eds. R. Melgar, Magen, H. & Lavado, R. INTA-IPI.

Morrás, H. & Delaune, M., 1985. Caracterización de áreas sedimentarias del norte de la Provincia de Santa Fe en base a la composición mineralógica de la fracción arena, *Ciencia del Suelo,* **3,** 140–151.

Morrás, H., Nabel, P. & Zech, W., 1998a. Identificación de distintos materiales parentales de suelos Argiudoles en un sector de la Pampa Ondulada (Castelar, Pcia. de Buenos Aires). Resúmenes, in *XVI Congreso Argentino de la Ciencia del Suelo,* pp. 305–306, Carlos Paz.

Morrás, H., Zech, W. & Nabel, P., 1998b. Composición geoquímica de suelos y sedimentos loéssicos de un sector de la Pampa Ondulada. Actas, in *V*

Jornadas Geológicas y Geofísicas Bonaerenses, Vol. I, pp. 225–232, Mar del Plata.

Morrás, H., Altinier, M., Castiglioni, M., Grasticini, C., Ciari G. & Cruzate, G. 2002. Composición mineralógica y heterogeneidad espacial de sedimentos loéssicos superficiales en la Pampa Ondulada, *Actas XVIII Reunión Argentina de la Ciencia del Suelo,* 4 p., Puerto Madryn (in CD-ROM).

Morrás, H., Altinier, M., Castiglioni, M. & Tessier, D., 2004a. Relación entre la mineralogía de arcillas y la susceptibilidad magnética en tres suelos del sur de la Pampa Ondulada, *Actas XIX Congreso Argentino de la Ciencia del Suelo,* Paraná, (in CD-Rom).

Morrás, H., Ciari, G., Grasticini, C., Cruzate, G., Altinier, M. & Castiglioni, M., 2004b. Variación espacial y relación entre la retención de humedad y la mineralogía magnética en suelos de la Pampa Ondulada, *Actas XIX Congreso Argentino de la Ciencia del Suelo,* Paraná, (in CD-Rom).

Morrás, H., Moretti, L., Píccolo, G. & Zech, W., 2009. About the genesis of subtropical soils with stone layers in NE Argentina. Autochthony and polygenesis, *Quat. Int.,* **196,** 137–159.

Moskowitz, B.M., Jackson, M.J. & Kissel, C., 1998. Low-temperature magnetic behavior of titanomagnetites, *Earth planet. Sci. Lett.,* **157,** 141–149.

Mullins, C.E., 1977. Magnetic susceptibility of the soil and its significance in soil science: a review, *J. Soil Sci.,* **28,** 223–246.

Mullins, C.E. & Tite, M.S., 1973. Magnetic viscosity, quadrature susceptibility, and frequency dependence of susceptibility in single-domain assemblies of magnetite and maghemite, *J. geophys. Res.,* **78,** 804–809.

Nabel, P.E., Morrás, H.J.M., Petersen, N. & Zech, W., 1999. Correlation of magnetic and lithologic features of soils and Quaternary sediments from the Undulating Pampa, Argentina, *J. South Am. Earth Sci.,* **12,** 311–323.

Oldfield, F., Maher, B.A., Donoghue, J. & Pierce, J., 1985. Particle-size related, mineral magnetic source-sediment linkages in the Rhode River catchment, Maryland, USA, *J. Geol. Soc. Lond.,* **142,** 1035–1046.

Olson, R.V. & Ellis, R., Jr., 1982. Iron, *Methods of Soil Analysis. Part 2. 2nd Ed. Chemical and Microbiological Properties,* pp. 301–312, ed A. L. Page *et al*., American Society of Agronomy and Soil Science Society of America, Madison, WI.

Orgeira, M.J. & Compagnucci, R., 2006. Correlation between paleosol-soil magnetic signal and climate, *Earth Planet. Space,* **58,** 1373–1380.

Orgeira, M.J., Walther, A.M., Vásquez, C.A., Tommaso, I.D.I., Alonso, S., Sherwood, G., Hu, Y.G. & Vilas, J.F.A., 1998. Mineral magnetic record of paleoclimate variation in loess and paleosol from the Buenos Aires formation (Buenos Aires, Argentina), *J. South Am. Earth Sci.,* **11,** 561–570.

Orgeira, M.J., Walther, A.M., Tófalo, R.O., Vásquez, C., Berquó, T., Favier Dobois, C. & Böhnel, H., 2003. Environmental magnetism in fluvial and loessic Holocene sediments and paleosols from the Chacopampean plain (Argentina), *J. South Am. Earth Sci.,* **16,** 259–274.

Orgeira, M.J., Pereyra, F.X., Vásquez, C., Castañeda, E. & Compagnucci, R., 2008. Rock magnetism in modern soils, Buenos Aires Province, Argentina, *J. South Am. Earth Sci.,* **26,** 217–224.

Özdemir, Ö., Dunlop, D.J. & Moskowitz, B.M., 1993. The effect of oxidation on the Verwey transition in magnetite, *Geophys. Res. Lett.,* **20,** 1671–1674.

Radhakrishnamurthy, C. & Likhite, S.D., 1993. Frequency dependence of low-temperature susceptibility peak in some titanomagnetites, *Phys. Earth Planet. Inter.,* **76,** 131–135.

Shi, C.D., Zhu, R.X., Suchy, V., Zeman, A., Guo & Pan, Y.X., 2001. Identification and Origins of Iron Sulfides in Czech Loess, *Geophys. Res. Lett.,* **28,** 3903–3906.

Simša, Z., Zounová, F. & Krupička, S., 1985. Initial permeability of single-crystal magnetite and Mn-ferrite, *Czech J. Phys.,* **35,** 1271–1281.

Singer, M.J., Bowen, L.H., Verosub, K.L., Fine, P. & TenPas, J., 1995. Mössbauer spectroscopic evidence for citrate-bicarbonate-dithionite extraction of maghemite from soils, *Clays Clay Miner.,* **43,** 1–7.

Skumryev, V., Blythe, H.J., Cullen, J. & Coey, J.M.D., 1999. AC susceptibility of a magnetite crystal, *J. Magn. Magn. Mater.,* **196–197,** 515–517.

Soil Survey Staff, 1999. Soil Taxonomy, in *A basic system for soil classification for making and interpreting soil surveys,* 2nd ed., 871 p., *Agricultural Handbook No. 436*, USDA, NRCS, Washington, DC.

Stephenson, A., 1971. Single domain grain distributions I. A method for the determination of single domain grain distributions, *Phys. Earth Planet. Inter.,* **4,** 353–360.

Sun, W., Banerjee, S.K. & Hunt, C.P., 1995. The role of maghemite in the enhancement of magnetic signal in the Chinese loess-paleosol sequence: an extensive rock magnetic study combined with citratebicarbonate-dithionite treatment, *Earth planet. Sci. Lett.,* **133,** 493–505.

Teruggi, M.E., 1957. The nature and origin of Argentina loess, *J. Sediment. Petrol.,* **27,** 322–332.

Torrent, J., Liu, Q.S., Bloemendal, J. & Barrón, V., 2007. Magnetic enhancement and iron oxides in the Upper Luochuan loess–paleosol sequence, Chinese Loess Plateau, *Soil Sci. Soc. Am. J.,* **71,** 1570–1578.

Torrent, J., Liu, Q.S. & Barrón, V., 2010. Magnetic minerals in Calcic Luvisols (Chromic) developed in a warm Mediterranean region of Spain: origin and paleoenvironmental significance, *Geoderma,* **154,** 465–472.

van Oorschot, I.H.M. & Dekkers, M.J., 1999. Dissolution behaviour of fine-grained magnetite and maghemite in the citratebicarbonate- dithionite extraction method, *Earth planet. Sci. Lett.,* **167,** 283–295.

van Velzen, A.J. & Dekkers, M.J., 1999. Low-temperature oxidation of magnetite in loess–paleosol sequences: a correction of rock magnetic parameters, *Stud. Geophys. Geod.,* **43,** 357–375.

Vasquez, C.A., Orgeira, M.J. & Sinito, A.M., 2009. Origin of superparamagnetic particles in Argiudolls developed on loess, Buenos Aires (Argentina), *Environ. Geol.,* **56,** 1653–1661.

Verosub, K.L., Fine, P., Singer, M.J. & TenPas, J., 1993. Pedogenesis and paleoclimate: interpretation of the magnetic susceptibility record of Chinese loess-paleosol sequences, *Geology,* **21,** 1011–1014.

Vidic, N.A., TenPas, J.D., Verosub, K.L. & Singer, M.J., 2000. Separation of pedogenic and lithogenic components of magnetic susceptibility in the Chinese loess/palaeosol sequence as determined by the CBD procedure and mixing analysis, *Geophys. J. Int.,* **142,** 551–562.

Volkov, I.A. & Zykina, V.S., 1982. Stratigraphy of the Quaternary loess deposits of the Novosibirsk Priobie, in *Proceedings of the 11th INQUA-Congree* ed. Arkhipov, V, S., Novosibirsk, *Russ. Acad. Sci.,* **82,** 17–21 (in Russian).

Worm, H.-U., 1998. On the superparamagnetic-stable single domain transition for magnetite, and frequency dependency of susceptibility, *Geophys. J. Int.,* **133,** 201–206.

Worm, H.-U. & Jackson, M., 1999. The superparamagnetism of Yucca Mountain Tuff, *J. geophys. Res.,* **104,** 25415–25425.

Zárate, M., 2003. Loess of southern South America, *Quat. Sci. Rev.,* **22,** 1987–2006.

Zhou, L.P., Oldfield, F., Wintle, A.G., Robinson, S.G. & Wang, J.T., 1990. Partly pedogenic origin of magnetic variations in Chinese loess, *Nature,* **346,** 737–739.